THE JOURNAL OF PHYSICAL CHEMISTRY B

Article

pubs.acs.org/JPCB

Highly Conductive Plastic Crystals Based on Fluorohydrogenate Anions

Ryosuke Taniki,[†] Kazuhiko Matsumoto,*[,†] Rika Hagiwara,[†] Kan Hachiya,[†] Takashi Morinaga,[‡] and Takaya Sato[‡]

[†]Graduate School of Energy Science, Kyoto University, Sakyo-ku, Kyoto 606-8501, Japan

[‡]Department of Chemical and Biological Engineering, Tsuruoka National College of Technology, 104 Sawada, Inooka, Tsuruoka 997-8511, Japan

Supporting Information

ABSTRACT: The new ionic plastic crystals *N*,*N*-dimethylpyrrolidinium fluorohydrogenate [DMPyr$(FH)_2F$] and *N*-ethyl-*N*-methylpyrrolidinium fluorohydrogenate [EMPyr$(FH)_2F$] were prepared, and their physicochemical, structural, and electrochemical properties were investigated. The DMPyr$(FH)_2F$ and EMPyr$(FH)_2F$ salts exhibited small entropy changes of melting, 4.1 and 2.0 J K^{-1} mol^{-1}, respectively, and had ionic plastic crystal phases in the temperature ranges of 258−325 and 236−303 K, respectively. These phases had NaCl-type structures; the lattice constants were 9.90 Å for DMPyr$(FH)_2F$ and 10.18 Å for EMPyr$(FH)_2F$. The ionic conductivities of the ionic plastic crystal phases ranged from 10^0 to 10^1 mS cm^{-1} [e.g., 10.3 mS cm^{-1} at 298 K for DMPyr$(FH)_2F$ and 14.4 mS cm^{-1} at 288 K for EMPyr$(FH)_2F$]. Pulsed-field gradient spin−echo NMR spectroscopy revealed that only the anion could move in the ionic plastic crystal phase as a charge carrier with a diffusion coefficient of $\sim10^{-7}$ cm^2 s^{-1}. The self-diffusion coefficient of the cation in the ionic plastic crystal phase of DMPyr$(FH)_2F$ was too small to measure, although the cation in EMPyr$(FH)_2F$ had a slight mobility below 303 K.

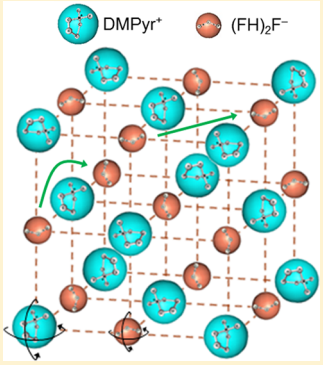

INTRODUCTION

Plastic crystals (PCs) are intermediate states formed below a material's melting point. The constituent species begin rotating by first-order solid−solid phase transitions from the crystal to the PC phase with large entropy changes. The entropy change corresponding to rotational freedom is thus very small in the transition from the PC to the liquid phase, which leads to a small entropy change of fusion (ΔS_{fus} < 20 J K^{-1} mol^{-1} for molecular PCs).[1] The rotating motion induces the diffusion of doped ions or a matrix, which enables the use of PCs as a new type of solid-state electrolyte.[2−4] For example, the rotation of SO_4^{2-} in the PC phase of Li_2SO_4 (848−1133 K) facilitates the diffusion of Li^+ through a paddle-wheel mechanism, resulting in substantial ionic conductivity (~1 S cm^{-1} at around 1000 K).[4,5] However, PCs that appear at high temperatures are difficult to handle, and material choice is limited. In contrast, organic materials often exhibit PC phases at lower temperatures. Organic molecular PCs can exhibit a certain degree of ionic conductivity originating solely from the doping of a salt in the nonionic matrix and can work well as solid-state electrolytes for electrochemical devices;[6−11] however, such systems have potential flammability and volatility issues. For example, a molecule of succinonitrile ($NCCH_2CH_2CN$) has high polarity and dissolves various types of salts in the PC phase at around room temperature.[6−8] Meanwhile, the study of ionic PCs (IPCs) has been increasingly extended, with progress in the chemistry of ionic liquids (ILs). Whereas organic salts based on pyrrolidinium and tetraalkylammonium cations often form low-melting ILs, those with short alkyl chains sometimes have an IPC phase at around room temperature.[3,12] The organic IPCs entirely consist of ions and, thus, have some benefits, such as nonflammability and low vapor pressures, that improve the safety and reliability of electrochemical devices. For example, the IPC *N*-ethyl-*N*-methylpyrrolidinium bis(trifluoromethylsulfonyl)amide (EMPyrTFSA) was studied as a solid-state electrolyte for lithium batteries. Although the ionic conductivity of the IPC phase of EMPyrTFSA in the neat form was 10^{-4} mS cm^{-1} at 333 K, the addition of a lithium salt (5 mol % LiTFSA) increased the ionic conductivity by several orders of magnitude to 2 × 10^{-1} mS cm^{-1} at 333 K.[2,13] Although solid-state ionic conductivities of 10^{-3}−10^0 mS cm^{-1} at room temperature have been achieved for some IPCs with additives,[3,6,12] further improvements in ionic conductivity would lead to a lower internal resistance in practical applications.

The IL 1-ethyl-3-methylimidazolium fluorohydrogenate [EMIm$(FH)_{2.3}F$] has a high ionic conductivity of 100 mS cm^{-1} and a low viscosity of 4.9 cP at 298 K, as well as a low melting temperature of 208 K.[14,15] In addition, the dissociation pressure of this IL is negligible at 298 K (<1 Pa). Fluorohydrogenate anions [$(FH)_nF^-$] are oligomeric complex ions, in which several HF units are bound as ligands to the

Received: November 23, 2012
Revised: December 27, 2012
Published: December 27, 2012

   dx.doi.org/10.1021/jp311558h | J. Phys. Chem. B 2013, 117, 955−960

central fluorine atom, and have been identified in various inorganic and organic salts.[16,17] Following the report of $EMIm(FH)_{2.3}F$, a series of fluorohydrogenate ILs with various cations were prepared. They exhibited lower viscosities and 1-order-of-magnitude higher ionic conductivities than ILs with the corresponding cation combined with other typical anions (e.g., 13 mS cm^{-1} and 34 cP for $EMImBF_4$).[18−20] The use of fluorohydrogenate ILs as electrolytes in electrochemical devices and processes has also been explored because of the unique functionality of $(FH)_nF^-$. The results of these previous studies motivated us to incorporate fluorohydrogenate anions into IPCs for application as solid-state electrolytes with high ionic conductivities.[21] The combination of the tetraethylphosphonium cation and fluorohydrogenate anion exhibited an IPC phase with an inverse nickel−arsenide-type structure and an ionic conductivity of 5 mS cm^{-1} at 323 K.[21] In the present study, the physicochemical, structural, and electrochemical properties of new IPCs composed of $(FH)_2F^-$ and *N*,*N*-dimethylpyrrolidinium ($DMPyr^+$) or *N*-ethyl-*N*-methylpyrrolidinium cations ($EMPyr^+$) (see Figure 1 for structures) are reported.

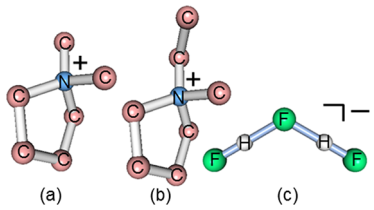

Figure 1. Structures of (a) $DMPyr^+$, (b) $EMPyr^+$, and (c) $(FH)_2F^-$. The hydrogen atoms in the cations are omitted for clarity.

EXPERIMENTAL SECTION

General Experimental Procedure. Volatile materials were handled using a vacuum line constructed of SUS316 stainless steel and tetrafluoroethylene−perfluoroalkylvinylether copolymer (PFA). Nonvolatile materials were handled in a glovebox under a dry Ar atmosphere. Chloromethane (Sumitomo Seika Chemicals, >99%) and *N*-methylpyrrolidine (Aldrich, 97%) were used as supplied. Acetonitrile (Wako Chemicals, 99%), ethyl acetate (Wako Chemicals, 99.5%), and ethanol (Wako Chemicals, 99.5%) were dried over molecular sieves and distilled just prior to use. *N*,*N*-Dimethylpyrrolidinium chloride (DMPyrCl) was prepared in the same manner as reported previously[18] and was purified by recrystallization from ethanol solution by adding ethyl acetate. *N*-Ethyl-*N*-methylpyrrolidinium chloride (EMPyrCl, Yoyulabo) was purified by recrystallization from acetonitrile solution by adding ethyl acetate. After recrystallization, the salts were dried under a vacuum at 393 K for 48 h. Aqueous NaOH solution (0.1965 M, Sigma-Aldrich) for titration was used as supplied. Anhydrous HF (Daikin Industries Co. Ltd., >99%) was dried over K_2NiF_6 prior to use. Handling of anhydrous HF was carefully performed using appropriate protective gear with immediate access to proper treatment procedures in case of accidental contact with liquid HF, HF vapor, or HF-containing compounds.[22,23]

Synthesis of $DMPyr(FH)_{2.0}F$. A large excess of anhydrous HF (aHF) was distilled onto DMPyrCl (29.80 g, 219.9 mmol) in a PFA reactor at 77 K, and unreacted HF and byproduct HCl were then eliminated at 298 K. Addition and elimination of aHF were repeated several times for effective elimination of chloride in the form of HCl. Final evacuation at 298 K below 1 Pa for several days gave $DMPyr(FH)_2F$ (35.12 g, 220.0 mmol). Testing for the presence of residual Cl^- with aqueous $AgNO_3$ solution gave no silver halide precipitation. The HF composition of 2.0 was confirmed by titration using aqueous NaOH solution. IR (AgCl): ν = 2323 (m), 1989 (m), 1811 (s), 1044 (w) cm^{-1} [$(FH)_2F^-$ in Figure S1 (Supporting Information)]. See refs 17 and 24 for the assignments of the IR bands.

Synthesis of $EMPyr(FH)_{2.0}F$. A large excess of aHF was distilled onto EMPyrCl (21.11 g, 134.5 mmol) in a PFA reactor at 77 K, and unreacted HF and byproduct HCl were then eliminated at 298 K. Addition and elimination of aHF were repeated several times for effective elimination of chloride in the form of HCl. Final pumping at 298 K below 1 Pa for several days gave $EMPyr(FH)_{2.3}F$ (24.10 g, 134.5 mmol). Removal of HF from $EMPyr(FH)_{2.3}F$ (4.61 g, 25.7 mmol) at 353 K in a PFA reactor gave $EMPyr(FH)_{1.8}F$ (4.35 g, 25.7 mmol). The fluorohydrogenate salt, $EMPyr(FH)_2F$, was prepared by mixing $EMPyr(FH)_{2.3}F$ and $EMPyr(FH)_{1.8}F$ in a molar ratio of 2 to 3. The HF composition of 2.0 was confirmed by titration using aqueous NaOH solution. Testing for the presence of residual Cl^- with aqueous $AgNO_3$ solution gave no silver halide precipitation. IR (AgCl): ν = 2326 (m), 1992 (m), 1810 (s), 1034 (w) cm^{-1} [$(FH)_2F^-$ in Figure S1 (Supporting Information)]. See refs 17 and 24 for the assignments of the IR bands.

Analysis. Thermal analysis was performed by differential scanning calorimetry (DSC) (Shimadzu DSC-60) and thermogravimetry (TG) (Shimadzu DTG-60H). For DSC, the samples were sealed in a pressure-resistant cell made of stainless steel under a dry argon atmosphere. Approximately 20 mg of the samples was loaded in the cell to avoid missing transitions with small exothermic or endothermic heats, such as that from the IPC phase to the IL phase. The samples were cooled to 133 K and heated above their melting points at 5 K min^{-1}. For TG, the samples, in a nickel cell, were heated to 573 K under a flow of dry argon at 10 K min^{-1}.

Samples for X-ray diffraction (XRD) were transferred into a quartz capillary under a dry argon atmosphere. The capillary was flame-sealed using an oxygen burner and was centered on an X-ray diffractometer (R-axis Rapid II, Rigaku) equipped with an imaging plate area detector (using the program RAPID XRD 2.3.3[25]) and monochromatized Mo Kα radiation (0.71073 Å). The φ angle was rotated at a rate of 1° s^{-1}, and the ω and χ angles were fixed at 20° and 0°, respectively, during data collection (1440 s). The sample temperature was controlled using a nitrogen gas flow. The targeting temperature was set according to the DSC results.

Ionic conductivity was measured by an ac impedance technique using a calibrated cell with platinum disk electrodes, with the aid of a Princeton Applied Research PARSTAT 2273 electrochemical measurement system. The cell was entirely filled with the liquefied sample at a temperature above its melting point prior to the measurement. The ionic conductivity data were measured after the sample was held at the target temperature for at least 1 h. The steadiness of the ionic conductivity value was confirmed by plotting it against time during this period.

Diffusion coefficients were measured by pulsed-field gradient spin−echo nuclear magnetic resonance (PGSE-NMR) spectroscopy using a JEOL JEM-ECX400 spectrometer. The

dx.doi.org/10.1021/jp311558h | J. Phys. Chem. B 2013, 117, 955−960

attenuation as a result of free diffusion in the Stejskal–Tanner sequence using half-sine-shaped gradient pulses was given by

$$E = S/S_0 = \exp[-\gamma^2 g^2 \delta^2 D(4\Delta - \delta)/\pi^2]$$

where γ is the gyromagnetic ratio, S is the amplitude of the echo signal, S_0 is the amplitude at which $g = 0$, g is the amplitude of the gradient pulse, δ is the duration of the gradient pulse, and Δ is the interval between the gradient pulses. Thus, D could be determined from the slope of the plot of ln E against varying g. In the present experiments, the maximum g value was 13.5 T/m, Δ was set to 10 ms, and the δ values were varied in the range of 0.1–1 ms.

Electrochemical stability was investigated by linear sweep voltammetry under a dry argon atmosphere with the aid of a Hokuto Denko HZ-3000 electrochemical measurement system. Vitreous carbon electrodes were used for the working and counter electrodes. A silver wire immersed in $EMImBF_4$ containing 0.05 M $AgBF_4$ was used for the reference electrode, which was partitioned from the electrolyte with a porous polytetrafluoroethylene (PTFE) filter (POREX, 7-μm pores).

RESULTS AND DISCUSSION

Thermal Behavior. Figure 2 shows the TG curves of $DMPyr(FH)_2F$ and $EMPyr(FH)_2F$. The weight losses above

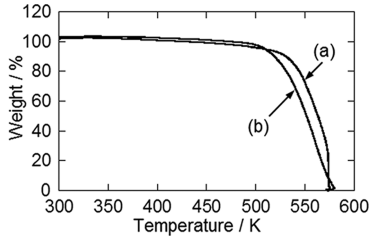

Figure 2. Thermogravimetric curves for (a) $DMPyr(FH)_2F$ and (b) $EMPyr(FH)_2F$. Scan rate = 10 K min^{-1}.

300 K in the TG curves are caused by the reversible elimination of HF from $(FH)_2F^-$. Irreversible decomposition of the cation is observed above 500 K. The high nucleophilicity of fluorohydrogenate anions results in lower decomposition temperatures compared to other dialkylpyrrolidinium salts.[26] Figure 3 shows DSC thermograms of $DMPyr(FH)_2F$ and $EMPyr(FH)_2F$ during the heating process (see Figure S2 in the Supporting Information for the entire DSC thermogram). The $DMPyr(FH)_2F$ salt exhibits a solid–solid phase transition (258

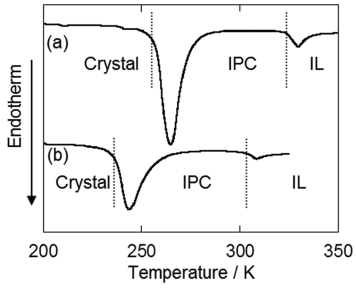

Figure 3. Differential scanning calorimetric curves for (a) $DMPyr(FH)_2F$ and (b) $EMPyr(FH)_2F$. ΔH = 14.7 kJ mol^{-1} at 258 K (crystal to IPC) and 1.3 kJ mol^{-1} at 325 K (IPC to IL) for $DMPyr(FH)_2F$. ΔH = 9.9 kJ mol^{-1} at 236 K (crystal to IPC) and 0.6 kJ mol^{-1} at 303 K (IPC to IL) for $EMPyr(FH)_2F$.

K) and melting point (325 K) during the heating process and a corresponding solid–solid phase transition (227 K) and freezing point (322 K) during the cooling process. The $EMPyr(FH)_2F$ salt exhibits a solid–solid phase transition (236 K) and melting point (303 K) during the heating process, whereas the cooling process shows two solid–solid phase transitions (210 and 167 K) and a freezing point (296 K) [see the Supporting Information for the solid phase of $EMPyr(FH)_2F$ observed between 210 and 167 K during the cooling process]. The ΔS_{fus} values of $DMPyr(FH)_2F$ (4.1 J K^{-1} mol^{-1}) and $EMPyr(FH)_2F$ (2.0 J K^{-1} mol^{-1}) are smaller than those of other IPCs [cf. 40 J K^{-1} mol^{-1} for EMPyrTFSA, 7.4 J K^{-1} mol^{-1} for $N_{1223}CF_3BF_3$ (N_{1223} = diethylmethylpropylammonium)].[1−3,12,21,26,27] Considering the soft textures of $DMPyr(FH)_2F$ and $EMPyr(FH)_2F$, in addition to the small ΔS_{fus} values, the IPCs are formed between the solid–solid and solid–liquid phase transitions [258–325 K for $DMPyr(FH)_2F$ and 236–303 K for $EMPyr(FH)_2F$ in the heating process]. Both salts have a small degree of supercooling in the phase transition from IL to IPC, because this phase transition has a small entropy change and solidification occurs easily. Both the crystal–IPC and IPC–IL phase transition temperatures for $DMPyr(FH)_2F$ are 22 K higher than those for $EMPyr(FH)_2F$. The difference is considered to be mainly derived from the different electrostatic interactions.

Structures. Panels a and b of Figure 4 show XRD patterns of the IPC phases of $DMPyr(FH)_2F$ and $EMPyr(FH)_2F$,

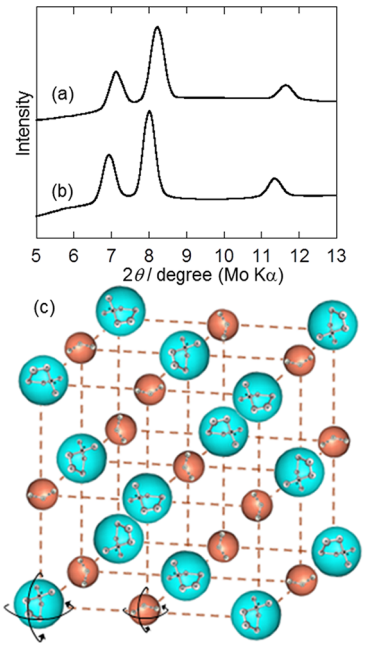

Figure 4. X-ray diffraction patterns of the IPC phases of (a) $DMPyr(FH)_2F$ and (b) $EMPyr(FH)_2F$ and (c) a schematic model of the IPC structure.

respectively. Figure 5 shows the XRD patterns of the crystal and IPC phases. In the XRD patterns of the IPC phases, only three diffraction peaks were observed in the low-2θ-angle region [7.11°, 8.24°, and 11.66° for $DMPyr(FH)_2F$; 6.98°, 8.01°, and 11.34° for $EMPyr(FH)_2F$]. The XRD peaks of the IPCs can be indexed with the indices (111), (200), and (220), as for a NaCl-type lattice, with lattice constants of 9.90 Å [$DMPyr(FH)_2F$] and 10.18 Å [$EMPyr(FH)_2F$] (see Figure 4c

dx.doi.org/10.1021/jp311558h | J. Phys. Chem. B 2013, 117, 955–960

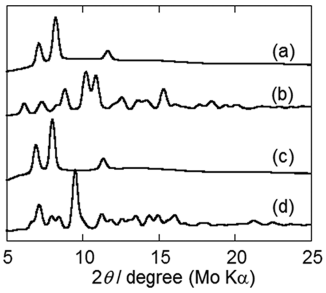

Figure 5. X-ray diffraction patterns of (a) the IPC phase of $DMPyr(FH)_2F$ at 298 K, (b) the crystal phase of $DMPyr(FH)_2F$ at 203 K, (c) the IPC phase of $EMPyr(FH)_2F$ at 263 K, and (d) the crystal phase of $EMPyr(FH)_2F$ at 183 K. All XRD patterns were obtained in the heating process.

for the IPC structure). The resulting lattice volume of the IPC phase for $DMPyr(FH)_2F$ (970 Å^3) is smaller than that for $EMPyr(FH)_2F$ (1055 Å^3), as a result of the smaller size of $DMPyr^+$ compared to $EMPyr^+$. The formation of a cubic lattice for the 1:1 IPC phase suggests that the ionic species (Figure 1) are rotating freely to form a large globular shape. This rapid rotating motion increases the thermal factors of the atoms in the lattice and prevents diffraction in the high-2θ-angle region. The increase in rotational degrees of freedom by the crystal–IPC phase transition results in more highly symmetric structures in the IPC phase. Similar behavior was observed for 1-ethyl-2-methylpyrrolinium TFSA and trimethylammonium trifluoroacetate by XRD,[28,29] the IPC phase of the latter being indexed as a CsCl-type cubic structure. The differences among structures with the IPC phases of the present pyrrolidinium $(FH)_2F^-$ salts (NaCl-type structure with a coordination number of six) and trimethylammonium trifluoroacetate (CsCl-type structure with a coordination number of eight) arise from the ratio of the cation size to the anion size; the trimethylammonium cation and trifluoroacetate anion have similar sizes, but $(FH)_2F^-$ is apparently smaller than $DMPyr^+$ or $EMPyr^+$, occupying the octahedral sites of the cations. It is noteworthy that the large tetraethylphosphonium cation forms an IPC phase with the hexagonal unit cell of the inverse nickel–arsenide-type structure when combined with $(FH)_2F^-$.[21]

Ionic Conductivity. Figure 6 shows Arrhenius plots of ionic conductivity for $DMPyr(FH)_2F$ and $EMPyr(FH)_2F$ (see Table 1 for ionic conductivity values). The discontinuous changes in ionic conductivity at the crystal–IPC and IPC–IL phase transitions agree with those observed by DSC. The ionic conductivities of the IPC phases range from 10^0 to 10^1 mS cm^{-1} [e.g., 10.3 mS cm^{-1} at 298 K for $DMPyr(FH)_2F$ and 14.4 mS cm^{-1} at 288 K for $EMPyr(FH)_2F$]. These values for $DMPyr(FH)_2F$ and $EMPyr(FH)_2F$ are higher than those of known IPCs in the neat form (e.g., 0.20×10^{-5} mS cm^{-1} at 298 K for DMPyrTFSA, 1.45×10^{-5} mS cm^{-1} at 298 K for EMPyrTFSA, 1.3×10^{-3} mS cm^{-1} at 313 K for *N,N′*-ringed pyrazolium TFSA, 1.9×10^{-3} mS cm^{-1} at 298 K for neat $N_{1223}CF_3BF_3$)[30,31] and in the salt-doped form (e.g., 2×10^{-1} mS cm^{-1} at 333 K for 5 mol % LiTFSA-doped EMPyrTFSA, 1.0×10^{-1} mS cm^{-1} at 313 K for 5 mol % LiTFSA-doped pyrazolium TFSA,[31] and 3.7×10^{-1} mS cm^{-1} at 298 K for 5 mol % $LiCF_3BF_3$-doped $N_{1223}CF_3BF_3$).[3] The activation energies obtained from the Arrhenius plots [4.4 and 7.6 kJ mol^{-1} for the IL and IPC phases, respectively, of $DMPyr(FH)_2F$; 4.9 and 8.6 kJ mol^{-1} for the IL and IPC phases, respectively, of $EMPyr(FH)_2F$] indicate that diffusion of the ions in the IPC phase has a larger energetic barrier than that in the IL phase. In the IL phase, $DMPyr(FH)_2F$ exhibits higher ionic conductivities (e.g., 138 mS cm^{-1} at 333 K) than $EMPyr(FH)_2F$ (e.g., 128 mS cm^{-1} at 333 K) because the smaller size of the cations results in a larger number of ions per volume, as in the cases of $DMIm(FH)_{2.3}F$ and $EMIm(FH)_{2.3}F$.[24] In the IPC phase, $DMPyr(FH)_2F$ exhibits lower ionic conductivities (e.g., 8.06 mS cm^{-1} at 288 K) than $EMPyr(FH)_2F$ (e.g., 14.4 mS cm^{-1} at 288 K).

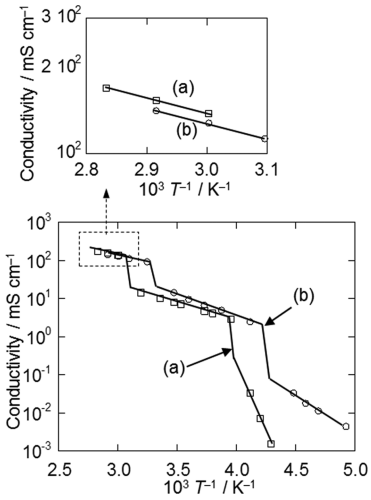

Figure 6. Arrhenius plots of ionic conductivity for (a) $DMPyr(FH)_2F$ and (b) $EMPyr(FH)_2F$.

Table 1. Ionic Conductivities (σ) of $DMPyr(FH)_2F$ and $EMPyr(FH)_2F$ at Different Temperatures

$DMPyr(FH)_2F$		$EMPyr(FH)_2F$	
T (K)	σ (mS cm^{-1})	T (K)	σ (mS cm^{-1})
353	170	343	142
343	154	333	128
333	139	323	113
313	14.3	308	91.1
298	10.3	288	14.4
288	8.06	278	9.38
283	7.12	268	6.87
268	4.70	258	4.98
256	4.09	243	2.46
253	2.89	223	0.034
243	0.034	218	0.018
238	0.007	213	0.011
233	0.002	203	0.0044

Diffusion Behavior. Figure 7 shows Arrhenius plots of self-diffusion coefficients for $DMPyr(FH)_2F$ and $EMPyr(FH)_2F$ obtained by PGSE-NMR spectroscopy (see Table S1 in the Supporting Information for the self-diffusion coefficient values). The self-diffusion coefficients of the cation and anion of $DMPyr(FH)_2F$ in the IL phase are 1.83×10^{-6} and 4.81×10^{-6} cm^2 s^{-1}, respectively, at 338 K. The self-diffusion coefficient of the anion of $DMPyr(FH)_2F$ in the IPC phase is 3.44×10^{-7} cm^2 s^{-1} at 298 K, whereas that of the cation was not measurable because of the small self-diffusion coefficient for $DMPyr^+$. These results suggest that the conductive species in the IPC phase of $DMPyr(FH)_2F$ is the anion. The difference between the self-diffusion coefficients of the IL and IPC phases is 1 order of magnitude and agrees with the difference between the

dx.doi.org/10.1021/jp311558h | J. Phys. Chem. B 2013, 117, 955–960

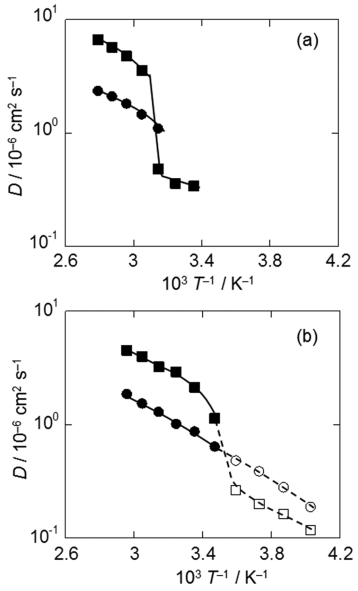

Figure 7. Arrhenius plots of self-diffusion coefficients for (a) $DMPyr(FH)_2F$ and (b) $EMPyr(FH)_2F$. Diffusion coefficients of the cation (●) and anion (■). The symbols ○ and □ indicate the diffusion coefficients of the cation and anion, respectively, in the IPC temperature range of $EMPyr(FH)_2F$.

ionic conductivities of these phases. The fact that only the anion is a charge carrier in the IPC phase indicates that the fluorohydrogenate IPC behaves as a superionic material.[32−35] The cation, without diffusion ability, holds the IPC lattice structure and supports the translation of the anion by rotating locally.

On the other hand, the diffusion behavior of the ionic species in the IPC temperature range of $EMPyr(FH)_2F$ is different from that of $DMPyr(FH)_2F$; the self-diffusion coefficient of $EMPyr^+$ can be measured even in the IPC-phase temperature range. This phenomenon is caused by a small number of mobile cations in the IPC lattice, because the peak intensity of $EMPyr^+$ gradually decreases with decreasing temperature [I_{cat}/I_{an} in the IPC phase is less than 10% of that in the IL phase, where I_{cat} and I_{an} at 255 K denote the peak intensities of $EMPyr^+$ and $(FH)_2F^-$]. It is noteworthy that this IL phase is not observed as a nonequilibrated phase, because the result is reproducible with increasing and decreasing temperatures and the time dependence showed that the peak intensity reached a steady state.

The different diffusion behaviors of $DMPyr(FH)_2F$ and $EMPyr(FH)_2F$ might be caused by the difference in the cationic structures. The IPC lattice of $EMPyr(FH)_2F$ has a looser packing than that of $DMPyr(FH)_2F$. This is supported by the low enthalpy change of melting and the broad peak for $EMPyr(FH)_2F$ in the DSC analysis, because of the lower symmetry of $EMPyr(FH)_2F$ compared to $DMPyr(FH)_2F$. As a result, some $EMPyr^+$ ions are mobile in the IPC lattice while the other cations hold the framework of the crystal lattice. In other words, in the case of $EMPyr(FH)_2F$, all of the cations do not necessarily remain stationary to form the crystal lattice. In the IPC-phase temperature range for $EMPyr(FH)_2F$, the self-diffusion coefficient of the cation is higher than that of the anion. The $EMPyr^+$ ions forming the crystal are not detected, as a result of low diffusivity, as for the cations in $DMPyr(FH)_2F$. However, mobile $EMPyr^+$ ions in the plastic crystal are detected and afford a high self-diffusion coefficient, for which the peak intensity in the IPC temperature range decreased as a result of the decrease in the number of mobile $EMPyr^+$ ions. Two kinds of anions are present in the $EMPyr(FH)_2F$ IPC phase: those that are strongly bound to the IPC lattice and those that are not. The former is dominant in the IPC phase, affording a low self-diffusion coefficient as an average value.

Ion Conduction Mechanism. It is unlikely that the anion migrates in the NaCl-type lattice in the form of $(FH)_2F^-$, because such an anion is too large to move in the lattice ($DMPyrBF_4$, with a similar anion size, does not show such a high ionic conductivity between 298 and 400 K[36,37]). As reported previously, the HF unit in $(FH)_nF^-$ exchanges between two anions in the IL state and functions as a dielectric spacer to weaken cation−anion interactions.[38] By analogy with this mechanism in the IL phase, the HF unit in $(FH)_2F^-$ in the IPC phase can act as a dielectric spacer between the cation and anion and facilitate the diffusion of the anion. Measurement of the diffusion behavior of fluorine nuclei was difficult in our experiments because of their long relaxation times. The existence of an isolated proton and the resulting proton hopping are not likely to occur under such basic conditions. Another important function of this HF exchange is the reduction of the effective anionic size.[38] In a very short period, $(FH)_2F^-$ in one site separates into two species, $(FH)_1F^-$ and the HF unit, and $(FH)_1F^-$ migrates in the shape of a rod through a narrow space to a neighboring site in the IPC (Figure 8). In the neighboring site, this $(FH)_1F^-$ unit catches the HF

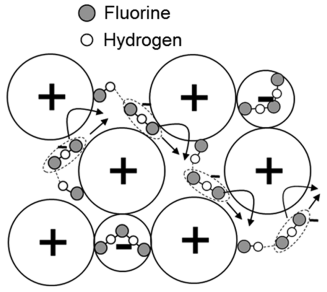

Figure 8. Possible ion conduction mechanism in the IPC phase of $DMPyr(FH)_2F$. The bent and straight arrows denote the diffusion paths of the anion along the [111] and [110] directions, respectively.

unit given by another $(FH)_2F^-$ to form a new $(FH)_2F^-$. These continuous phenomena [release of HF, migration of $(FH)_1F^-$, and capture of HF] can transfer the charge in the IPC (Figure 8), leading to the high ionic conductivity. The [111] direction is the most widely opened diffusion path for the anion, whereas the path directed along [110] is narrow but the shortest to the neighboring anion site.

Electrochemical Behavior. A linear sweep voltammogram of a vitreous carbon electrode in the IPC phase of $DMPyr(FH)_2F$ at 298 K (Figure 9) revealed that the anodic and cathodic currents were observed from +2.0 and −1.9 V (vs Fc^+/Fc), respectively. The electrochemical stability of the $DMPyr(FH)_2F$ IPC is similar to those observed for *N*-alkyl-*N*-methylpyrrolidinium fluorohydrogenate ionic liquids.[18] As mentioned in the previous study,[15] the reaction at the cathodic limit probably includes the reduction of both the cation and anion. The reaction at the anode limit is probably decomposition of the IPC, including fluorination of the cation.

dx.doi.org/10.1021/jp311558h | J. Phys. Chem. B 2013, 117, 955−960

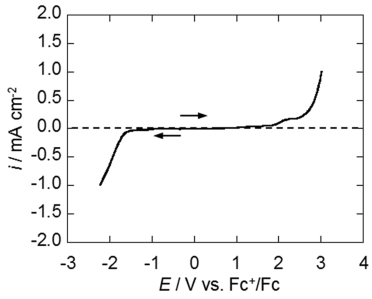

Figure 9. Linear sweep voltammogram of a vitreous carbon electrode in the IPC phase of DMPyr$(FH)_2F$ at 298 K.

CONCLUSIONS

New IPCs based on fluorohydrogenate anions were prepared, and their physicochemical, structural, and electrochemical properties were investigated. The fluorohydrogenate salts DMPyr$(FH)_2F$ and EMPyr$(FH)_2F$ have IPC phases in the temperature ranges of 258−325 and 236−303 K, respectively. These phases have NaCl-type structures and exhibit small entropy changes of melting. The ionic conductivities of the IPC phases are the highest known for IPC phases, ranging from 10^0 to 10^1 mS cm^{-1}. Pulsed-field gradient spin−echo NMR spectroscopy revealed that only the anion can move in the IPC phase as a charge carrier.

ASSOCIATED CONTENT

Supporting Information

IR spectra, DSC curves, XRD patterns, and diffusion coefficient values. This material is available free of charge via the Internet at http://pubs.acs.org.

AUTHOR INFORMATION

Corresponding Author

*Phone: +81 75 753 5822. Fax: +81 75 753 5906. E-mail: k-matsumoto@energy.kyoto-u.ac.jp.

Notes

The authors declare no competing financial interest.

ACKNOWLEDGMENTS

The authors thank The Hattori Houkou Foundation for financial support of this work.

REFERENCES

(1) Timmermans, J. *J. Phys. Chem. Solids* **1961**, *18*, 1.
(2) MacFarlane, D. R.; Huang, J.; Forsyth, M. *Nature* **1999**, *402*, 792.
(3) Zhou, Z.; Matsumoto, H. *Electrochem. Commun.* **2007**, *9*, 1017.
(4) Aronsson, R.; Jansson, B.; Knape, H. E. G.; Lundén, A.; Nilsson, L.; Sjöblom, C.-A.; Torell, L. M. *J. Phys. Colloq.* **1980**, *41*, C6.
(5) Dissanayake, M. A. K. L.; Mellander, B.-E. *Solid State Ionics* **1986**, *21*, 279.
(6) Alarco, P.-J.; Abu-Lebdeh, Y.; Abouimrane, A.; Armand, M. *Nat. Mater.* **2004**, *3*, 4761.
(7) Abouimrane, A.; Abu-Lebdeh, Y.; Alarco, P.-J.; Armand, M. *J. Electrochem. Soc.* **2004**, *151*, A1028.
(8) Long, S.; MacFarlane, D. R.; Forsyth, M. *Solid State Ionics* **2004**, *175*, 733.
(9) Patel, M.; Bhattacharyya, A. J. *Electrochem. Commun.* **2008**, *10*, 1912.
(10) Patel, M.; Chandrappa, K. G.; Bhattacharyya, A. J. *Electrochim. Acta* **2008**, *54*, 209.
(11) Das, S.; Bhadram, V. S.; Narayana, C.; Bhattacharyya, A. J. *J. Phys. Chem. B* **2011**, *115*, 12356.
(12) MacFarlane, D. R.; Meakin, P.; Sun, J.; Amini, N.; Forsyth, M. *J. Phys. Chem. B* **1999**, *103*, 4164.
(13) Forsyth, M.; Huang, J.; MacFarlane, D. R. *J. Mater. Chem.* **2000**, *10*, 2259.
(14) Hagiwara, R.; Hirashige, T.; Tsuda, T.; Ito, Y. *J. Electrochem. Soc.* **2002**, *149*, D1.
(15) Hagiwara, R.; Nakamori, Y.; Matsumoto, K.; Ito, Y. *J. Phys. Chem. B* **2005**, *109*, 5445.
(16) Cady, G. H. *J. Am. Chem. Soc.* **1934**, *56*, 1431.
(17) Gennick, I.; Harmon, K. M.; Potvin, M. M. *Inorg. Chem.* **1977**, *16*, 2033.
(18) Matsumoto, K.; Hagiwara, R.; Ito, Y. *Electrochem. Solid-State Lett.* **2004**, *7*, E41.
(19) Yamagata, M.; Konno, S.; Matsumoto, K.; Hagiwara, R. *Electrochem. Solid-State Lett.* **2009**, *12*, F9.
(20) Ohtsuki, J.; Matsumoto, K.; Hagiwara, R. *Electrochemistry* **2009**, *77*, 624.
(21) Enomoto, T.; Kanematsu, S.; Tsunashima, K.; Matsumoto, K.; Hagiwara, R. *Phys. Chem. Chem. Phys.* **2011**, *13*, 12536.
(22) Matsumoto, K.; Hagiwara, R. *J. Fluorine Chem.* **2010**, *131*, 805.
(23) Peters, D.; Miethchen, R. *J. Fluorine Chem.* **1996**, *79*, 161.
(24) Hagiwara, R.; Matsumoto, K.; Nakamori, Y.; Tsuda, T.; ito, Y.; Matsumoto, H.; Momota, K. *J. Electrochem. Soc.* **2003**, *150*, D195.
(25) *RAPID XRD*, version 2.3.3; Rigaku Corporation: Tokyo, Japan, 1999.
(26) Forsyth, S. A.; Batten, S. R.; Dai, Q.; MacFarlane, D. R. *Aust. J. Chem.* **2004**, *57*, 121.
(27) Annat, G.; Adebahr, J.; McKinnon, I. R.; MacFarlane, D. R.; Forsyth, M. *Solid State Ionics* **2007**, *178*, 1065.
(28) Sun, J.; MacFarlane, D. R.; Forsyth, M. *Solid State Ionics* **2002**, *148*, 145.
(29) Kuchitsu, K.; Ono, H.; Ishimaru, S.; Ikeda, R.; Ishida, H. *Phys. Chem. Chem. Phys.* **2000**, *2*, 3883.
(30) Hill, A. J.; Huang, J.; Efthimiadis, J.; Meakin, P.; Forsyth, M.; MacFarlane, D. R. *Solid State Ionics* **2002**, *154−155*, 119.
(31) Alarco, P.-J.; Abu-Lebdeh, Y.; Ravet, N.; Armand, M. *Solid State Ionics* **2004**, *172*, 53.
(32) Harris, K. R. *J. Phys. Chem. B* **2010**, *114*, 957.
(33) Tasseven, Ç.; Trullàs, J.; Alcaraz, O.; Silbert, M.; Giró, A. *J. Chem. Phys.* **1997**, *106*, 7286.
(34) Hull, S. In *Solid State Electrochemistry*; I. Kharton, V. V., Ed.; Wiley-VCH Verlag: Weinheim, Germany, 2009; p 15.
(35) Anouti, M.; Caillon-Caravaner, M.; Dridi, Y.; Galiano, H.; Lemordant, D. *J. Phys. Chem. B* **2008**, *112*, 13335.
(36) Efthimiadis, J.; Forsyth, M.; MacFarlane, D. R. *J. Mater. Sci.* **2003**, *38*, 3293.
(37) Efthimiadis, J.; Pas, S. J.; Forsyth, M.; MacFarlane, D. R. *Solid State Ionics* **2002**, *154−155*, 279.
(38) Enomono, T.; Nakamori, Y.; Matsumono, K.; Hagiwara, R. *J. Phys. Chem. C* **2011**, *115*, 4324.